Electroactive protecting groups and reaction units. Part 4. Mesolytic O–CO bond cleavage *versus* intramolecular cyclization reaction in enol trifluoroacetate cation radicals. A kinetic and mechanistic investigation †

Michael Schmittel * and Holger Trenkle

Institut für Organische Chemie, Universität Würzburg, Am Hubland, D-97074 Würzburg, Germany

The one-electron oxidation of two β,β-dimesityl enol trifluoroacetates with different substituents R at C_α was investigated. For the first time enol trifluoroacetate cation radicals could be reversibly monitored in cyclic voltammetry experiments allowing the determination of the rate constants of their follow-up reactions. While mesolytic cleavage of the O–CO bond ($k_f = 1.4\ s^{-1}$) with direct formation of an α-carbonyl cation constitutes the primary reaction of the enol trifluoroacetate cation radical with R = Bu^t, the one with R = Ph exclusively cyclizes ($k_f = 75\ s^{-1}$) to a phenanthrene derivative. This change in reactivity can be rationalized by the different nature of the electrophoric system as a function of the substituent R.

Introduction

In many cases, activation barriers for bond dissociation processes are effectively decreased for cation radicals, which allows the use of one-electron oxidation in synthetic schemes as a powerful and selective method to break, *e.g.*, C–C, C–O and O–X bonds that are quite strong in neutral substrates.[1] In this context, mesolytic cleavage of O–X bonds in enol type cation radicals has recently attracted our interest,[2,3] since the highly selective deprotection of silyl enol ethers could be effected in the presence of alkoxysilanes after one-electron oxidation.[4]

Furthermore, the oxidative addition of enol derivatives to electron-rich olefins is a promising protocol to form C–C bonds under mild conditions.[5] Several mechanistic alternatives for this reaction are discussed in the literature, with either the bond formation taking place at the cation radical or the α-carbonyl radical stage (after mesolytic cleavage of the O–X bond). For a sound distinction between these two processes, information is needed on the kinetics of such mesolytic bond cleavage reactions in comparison with kinetics of nucleophilic attack on cation radicals.

In continuation of our earlier work,[2,3] we present herein the first kinetic and mechanistic investigations on mesolytic bond cleavage and cyclization processes in enol trifluoroacetate cation radicals. To monitor such reactions without interference, other typical processes, such as deprotonation in the γ-position and nucleophilic attack in the β-position of the enol ester cation radical, had to be rigorously excluded. Hence, the enol trifluoroacetates **T1** and **T2** were chosen as sterically hindered[2,6] model systems.

Results

Synthesis

The model compounds could be smoothly prepared from the corresponding enolates after esterification with trifluoroacetic anhydride in 77% (**T1**) and 80% (**T2**) yield, respectively. Notably, the ^{1}H NMR spectra of both enol trifluoroacetates exhibit interesting coalescence phenomena, probably due to a two or three-blade propeller conformation, caused by the hindered rotation of the mesityl groups as has already been shown for the 2,2-dimesityl-1-phenylethenol[7] and its dimethyl-*tert*-butylsilyl enol ether.[3a]

† For Part 3 see ref. 3*b*.

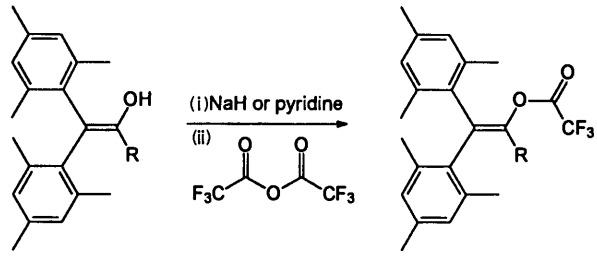

E1: R = Bu^t
E2: R = Ph

T1: R = Bu^t
T2: R = Ph

Scheme 1

Preparative one-electron oxidation

Preparative scale electrolysis of **T1** in acetonitrile–trifluoroacetic acid afforded in a clean reaction the known benzofuran **B1**[8] (32% yield) and unreacted **T1** (51%).‡ In contrast, the one-electron oxidation of **T2** with tris(4-nitrophenyl)aminium hexachloroantimonate or preparative scale electrolysis provided solely phenanthrene **PT2** as evidenced by the ^{1}H NMR data (Scheme 2). Unfortunately, **PT2** could not be separated from unreacted **T2** (conversion 65%).‡ Under conditions of column chromatography (SiO_2), however, or by treatment with ethanolic KOH, **PT2** was hydrolysed affording 9-hydroxy-10-mesityl-1,3,4-trimethylphenanthrene **P2** in 20% yield, the structure of which could unambiguously be established on the basis of the spectral data.

CV investigations

At a scan rate of 100 mV s^{-1} the enol trifluoroacetates **T** exhibited irreversible oxidation waves in acetonitrile, similar to those of the corresponding enol acetates **A** that had been investigated earlier.[2] However, in comparison with the latter, the anodic peak potentials E_{pa} of **T1** and **T2** were shifted anodically (Table 1).§

T1 displays a simple irreversible oxidation wave in acetonitrile at all scan rates ≤200 mV s^{-1} with decreasing $I_{pa}/v^{1/2}$

‡ To avoid further oxidation of the products, the electrolysis was stopped at partial conversion.

§ All potentials are referred to the ferrocene/ferrocenium (Fc) couple unless otherwise noted. To obtain values *vs.* SCE, simply add +0.39 V.

Table 1 Oxidation potentials of the enol trifluoroacetates, enol acetates, enols and benzofurans *vs.* Fc

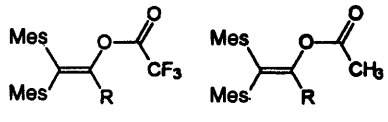

T1/T2 **A1/A2**

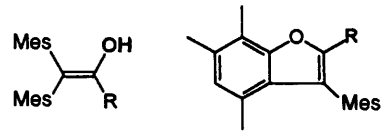

E1/E2 **B1/B2**

	T1/T2	A1/A2	E1/E2	B1/B2
1 R = Bu^t	E_{pa} = 1.51[a]	$E_{1/2}$ = 1.16[b,c]	$E_{1/2}$ = 0.73[b,d]	$E_{1/2}$ = 0.93[b,e]
2 R = Ph	E_{pa} = 1.26[a]	E_{pa} = 1.04[b,c]	$E_{1/2}$ = 0.67[b,d]	$E_{1/2}$ = 0.87[b,e]

[a] Irreversible peak potential at 100 mV s^{-1}, 0.001 M in acetonitrile/0.1 M Bu_4NPF_6. [b] Thermodynamic half-wave potential, 0.001 M in dichloromethane/0.1 M Bu_4NPF_6. [c] Ref. 2. [d] Ref. 11. [e] Ref. 15.

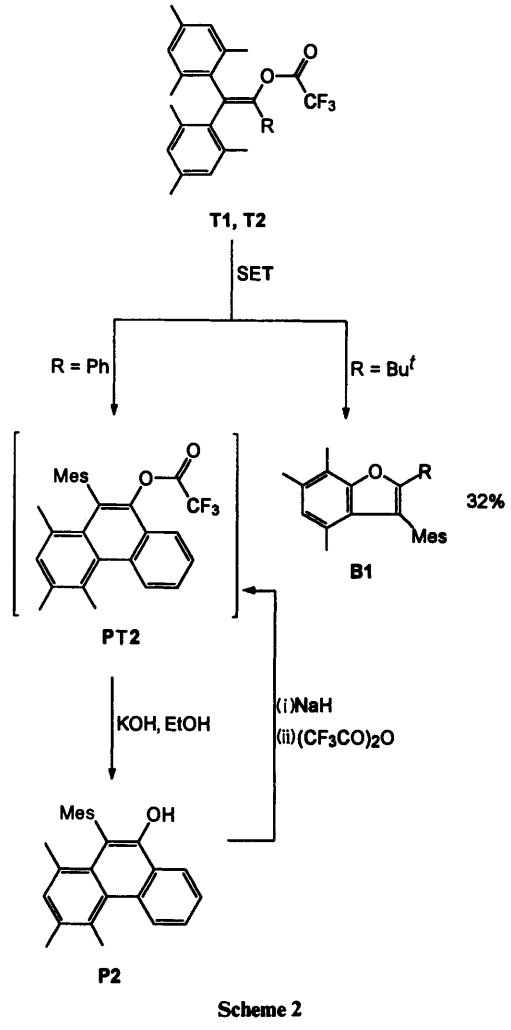

Scheme 2

when increasing *v*. Calibration against tris(*p*-bromophenyl)-amine revealed that the oxidation wave of **T1** corresponds to the transfer of only one electron. At a scan rate of 1 V s^{-1}, the oxidation wave turns partially reversible [Fig. 1(*a*)], allowing for a kinetic evaluation of the follow-up process using the Nicholson–Shain formalism.[9] Assuming an EC_{irr}-mechanism, the first-order rate constant could be determined as k_f = 1.4 s^{-1} at 0 °C in acetonitrile.

Cyclic voltammetry investigations of **T2** likewise provide an irreversible anodic wave (E_{pa} = 1.26 V), but in addition a reduction wave at E_{pc} = 1.10 V on the reverse scan. The latter wave cannot be caused by the reduction of **T2**$^{\bullet+}$ [Fig. 1(*b*)] and must therefore stem from a follow-up product. In multisweep experiments, an oxidation wave corresponding to the new reduction product emanated [Fig. 1(*c*)], but it is not completely separated from the oxidation wave of **T2**. A half-wave potential $E_{1/2}$ = 1.13 V was determined for the follow-up product. Digital simulation[10] of the multisweep experiment of **T2**, using an $ECECEC_{DISP}$ mechanism, showed a good coincidence with the experimental CV.

To probe whether the wave at $E_{1/2}$ = 1.13 V can be assigned to the trifluoroacetate **PT2**, it was prepared from **P2** with sodium hydride and trifluoroacetic anhydride. Comparison of its ^{1}H NMR and cyclic voltammetry data with those of the crude reaction mixture unequivocally established that **PT2** is the primary one-electron oxidation product of **T2**.

When using fast scan CV to probe the lifetime of **T2**$^{\bullet+}$, a new reduction wave corresponding to **T2**$^{\bullet+}$ + e$^-$ ⟶ **T2** could be detected at scan rates >20 V s^{-1} allowing us to estimate the first-order rate constant k_f = 75 s^{-1} for the follow-up reaction of **T2**$^{\bullet+}$.

Discussion

Oxidation potentials

Not unexpectedly, the oxidation potentials of **T1,T2** caused by the strongly electron-withdrawing effect of the trifluoroacetyl group, are markedly higher than those of other enol derivatives (see Table 1). However, when comparing enol acetates **A1,A2** and enol trifluoroacetates **T1,T2**, the incremental increase ΔE_{pa} is much smaller in the case of the phenyl substituted **T2**. This may be indicative of the fact that the electrophore system changes from the $Mes_2C{=}C{-}O$ moiety in **T1** to the $Mes_2C{=}C{-}Ph$ constituent in **T2**. Indeed, such an interpretation is supported by the different reactivity pattern of the corresponding cation radicals.

Mesolytic fragmentation of T1$^{\bullet+}$

Formation of benzofuran **B1** suggests that **T1**$^{\bullet+}$ undergoes O–CO bond cleavage analogous to the mesolytic fragmentations of enol acetate cation radicals[2] (Scheme 3). The alternative pathway, cyclization on the stage of **T1**$^{\bullet+}$ to a distonic cation radical that is further oxidized to a dication can be excluded since then we would expect the anodic wave to correspond to a two electron oxidation process, which is not the case.

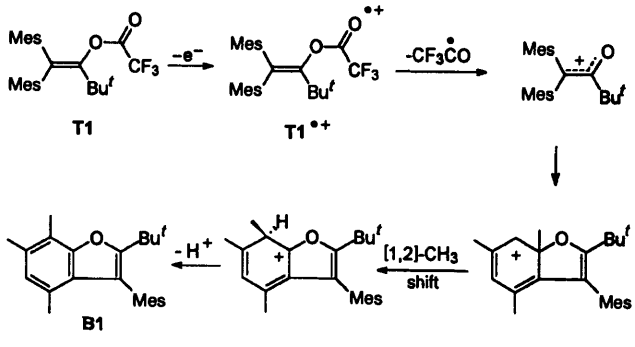

Scheme 3

We assume that mesolytic cleavage selectively provides the trifluoroacetyl radical and an α-carbonyl cation. The α-carbonyl cation then undergoes a fast Nazarov cyclization, followed by a slow [1,2]-methyl shift (Scheme 3) and deprotonation of the resulting cyclohexadienyl cation to afford benzofuran **B1** as the exclusive product of the one-electron oxidation of **T1**.

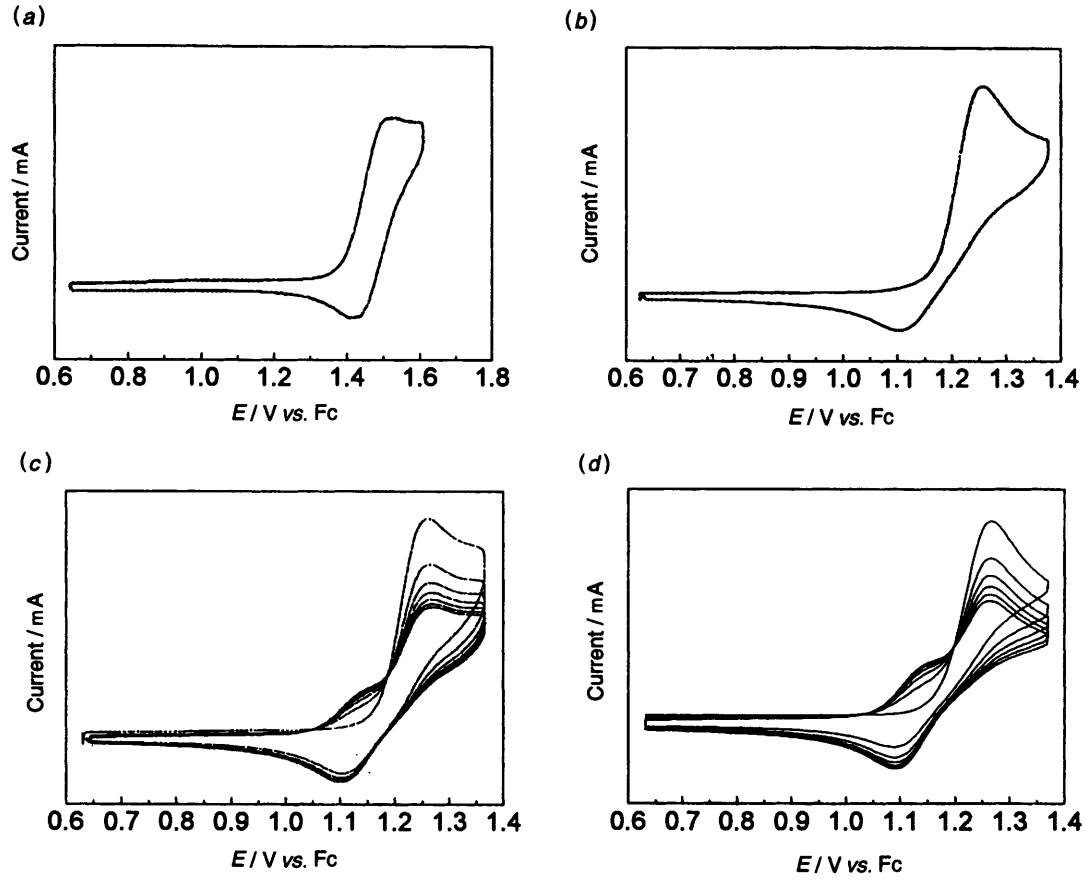

Fig. 1 CV of the enol trifluoroacetates and digital simulation. (*a*) CV of **T1**, 0.001 M in acetonitrile/0.1 M Bu_4NFP_6 at 1 V s^{-1}; (*b*) CV of **T2**, 0.001 M in acetonitrile/0.1 M Bu_4NPF_6 at 100 mV s^{-1}; (*c*) multisweep-experiment of **T2** at 500 mV s^{-1}; (*d*) digital simulation of (*c*).

Thermochemical cycle:

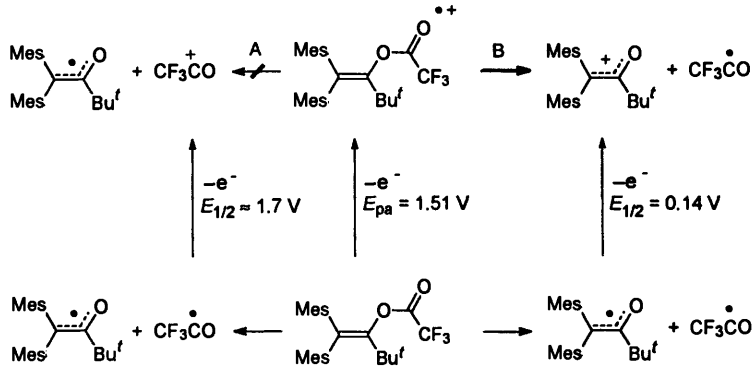

T1

Scheme 4

In principle, another plausible fragmentation selectivity, resulting in the formation of the corresponding α-carbonyl radical and a trifluoroacylium cation, could be postulated, which is, however, less favourable as derived from a thermochemical calculation (Scheme 4). Pathway B is favoured by 150 kJ mol^{-1}, since the oxidation potential of the α-carbonyl radical ($E_{1/2}$ = 0.14 V)[11] is much lower than that of the trifluoroacetyl radical ($E_{1/2}$ *ca.* 1.7 V). The latter was estimated using Miller's[12] or Gassman's[13] correlation of Ei_a *vs.* $E_{1/2}$ with the AM1 calculated adiabatic ionization potential of $CF_3CO^{\bullet}$ (Ei_a = 9.2 eV).[14]

In earlier investigations on the corresponding enol acetate cation radicals $\mathbf{A}^{\bullet+}$ it was unequivocally proved that the fragmentation follows the selectivity shown in Scheme 3. As the oxidation potential of the $CH_3CO^{\bullet}$ radical is lower than that of $CF_3CO^{\bullet}$ ($E_{1/2}$ *ca.* 1.1 V *vs. ca.* 1.7 V), the direct formation of an α-carbonyl cation intermediate is even more favoured thermodynamically in the O–CO bond fragmentation of enol trifluoroacetate cation radicals.

One-electron oxidation of T2

The occurrence of a reduction wave at E_{pc} = 1.10 V *vs.* Fc after oxidation of **T2** implies that a new follow-up product is formed on the timescale of the CV experiment. In earlier investigations,[2] a similar phenomenon was observed for the corresponding enol acetates **A1** and **A2**, which could be easily explained by the formation of benzofurans **B1** and **B2**. With **T2**, however, the reduction wave in the CV does not coincide with the redox potential of the corresponding benzofuran derivative **B2** ($E_{1/2}$ = 0.87 V *vs.* Fc),[11] which would be the anticipated product derived from mesolytic cleavage of the cation radical.[15] The reduction wave must be assigned to the reduction of $\mathbf{PT2}^{\bullet+}$ instead, formed from **T2** under anodic oxidation conditions.

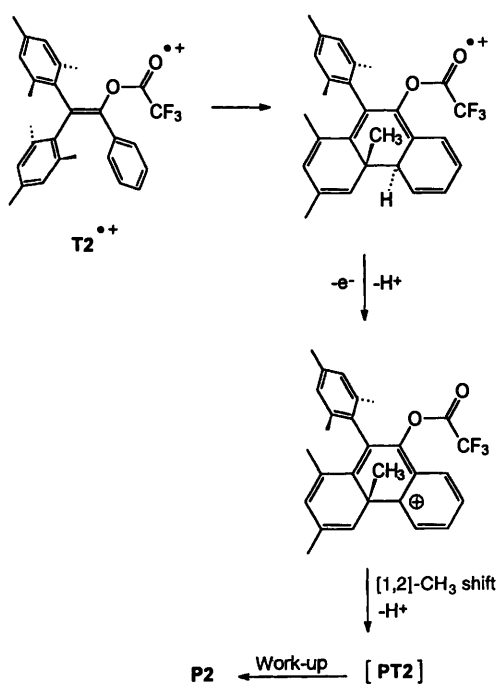

Scheme 5

Apparently, the mesolytic O–CO bond cleavage in $T2^{\bullet+}$ cannot compete with the much faster cyclization as shown in Scheme 5. After deprotonation, further oxidation of the resulting radical, [1,2]-methyl shift and deprotonation, **PT2** is formed and immediately oxidized at the applied working potential. As $PT2^{\bullet+}$ is sufficiently persistent, it is reduced in the CV and **PT2** accumulates in the diffusion layer. As a consequence, the corresponding oxidation wave can be observed in the multisweep experiment. The occurrence of isopotential points[16] indicates that one electroactive species was quantitatively converted into another, the sum of reactant and product concentration thus remaining constant.[17]

The multisweep CV trace could be successfully simulated using a $ECECEC_{DISP}$ mechanism¶ (Fig. 1) using k_f *ca.* 75–80 s^{-1} for the follow-up reaction of $T2^{\bullet+}$ and *k ca.* 3 s^{-1} for the second chemical step. In addition, the redox data of **PT2** were added to the simulation file.

Lifetime of the cation radicals

Knowing the homolytic O–CO bond dissociation energies‖ one can determine the mesolytic fragmentation of $A1^{\bullet+}$ to be more endergonic than that of $T1^{\bullet+}$ by 26 kJ mol^{-1}. This is a result of a straightforward thermochemical cycle calculation because $E_{pa}(T1) > E_{pa}(A1)$. Quite unexpectedly, however, $T1^{\bullet+}$ is more persistent by a factor of 10^4 in acetonitrile than the corresponding $A1^{\bullet+}$. Apparently, quite in contrast to C–C bond fragmentations in substituted bicumyl cation radicals,[19] there is no correlation between the thermochemical driving force and the kinetics. This behaviour can be readily rationalized in light of a three-electron two-orbital two-configuration model.[20] Accordingly, both $A1^{\bullet+}$ and $T1^{\bullet+}$ possess a Π-ground state, but the bond dissociation is governed by the relative energy of the Σ state, which is much less favourable with $T1^{\bullet+}$ because of the lower lying σ (O–$COCF_3$) (Fig. 2).

¶ 'E' stands for electrochemical, 'C' for chemical reaction step. For this type of reaction, the expression 'DISP' has been established in spite of the fact that this is not a disproportionation reaction but an electron-transfer equilibrium between the employed redox-active species.[18]

‖ Semiempirical AM1 calculations have revealed that the homolytic O–CO bond energies in vinylacetate and vinyltrifluoroacetate differ by less than 4.2 kJ mol^{-1}.

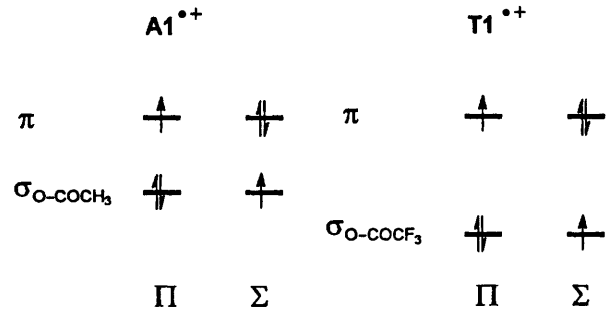

Fig. 2 Three-electron two-orbital two-configuration model of $A1^{\bullet+}$ and $T1^{\bullet+}$

Conclusion

Using cyclic voltammetry and preparative one-electron oxidation, it could be shown that two similar enol trifluoroacetates exhibit completely different follow-up reactions of their cation radicals. In addition, the mesolytic O–CO bond cleavage of enol trifluoroacetate cation radicals is much smaller than those of the corresponding enol acetate cation radicals although they are less endergonic. This behaviour has been rationalized in terms of the three-electron two-orbital two-configuration model.

Experimental

General aspects

250 MHz ^1H NMR and 150 MHz ^{13}C NMR spectra were recorded in $CDCl_3$ on a Bruker AC250 or a Bruker DMX600. Chemical shifts are reported in ppm downfield *vs.* the internal standard $SiMe_4$ and coupling constants are given in Hz. The abbreviation br designates signals broadened by coalescence. IR spectra were recorded in KBr using a Perkin-Elmer FTIR infrared spectrometer. Mass spectra were recorded on a Finnigan MAT 8200 Mass spectrometer using electron ionization (EI) at 70 eV. Elemental analyses were performed at the Institute for Inorganic Chemistry, University of Würzburg. Melting points were taken on a Büchi Smp-20 apparatus and are uncorrected.

Materials

Commercial reagents were purchased from standard chemical suppliers and were used without further purification. Acetonitrile for CV and one-electron oxidation was purchased in HPLC quality from Riedel-de-Haën, distilled over calcium hydride and filtered through basic alumina (ICN). The preparation of the corresponding enols has been reported elsewhere.[6]

General procedure for the preparation of the trifluoroacetates from the corresponding enols

Enol **E** (1.3–1.7 mmol) was suspended in trifluoroacetic anhydride (20 mmol), and pyridine was added dropwise until the enol had completely dissolved. After stirring for 24 h at room temp., the reaction mixture was poured on ice, 5% HCl (5 cm^3) was added, and the resulting suspension was extracted three times with diethyl ether. The combined organic layers were washed with saturated aqueous $NaHCO_3$ and water and dried over Na_2SO_4. Removal of the solvent and recrystallization from methanol at 8 °C afforded the pure enol trifluoroacetates as white solids.

1,1-Dimesityl-3,3-dimethyl-2-trifluoroacetoxybut-2-ene (T1). 1,1-Dimesityl-3,3-dimethylbut-1-en-2-ol (E1) (0.40 g, 1.2 mmol), pyridine (0.50 g, 6.3 mmol) and trifluoroacetic anhydride (1.3 g, 6.2 mmol) afforded 0.40 g (0.90 mmol, 77%) of **T1** as a white solid. Mp 127–130 °C (Found: C, 71.7; H, 7.75. $C_{26}H_{31}O_2F_3$ requires: C, 72.2; H, 7.2%). IR (KBr): ν_{max}/cm^{-1} = 2970 (C–H), 1770 (C=O), 1600 (C=C), 1470, 1360, 1220, 1150, 860. $\delta_H(CDCl_3)$ 1.06 [s, 9 H, $C(CH_3)_3$], 1.75–2.05 (br, 6 H, *o*-CH_3), 2.17 (s, 3 H, *p*-CH_3), 2.22 (s, 3 H, *p*-CH_3), 2.30–2.55 (br, 3 H, *o*-CH_3), 2.60–2.90 (br, 3 H, *o*-CH_3),

6.50–6.90 (br, 4 H, mesityl-H). δ_C($CDCl_3$, 150 MHz) 20.34, 28.10 [C(CH_3)$_3$], 38.67 [C(CH_3)$_3$], 114.39 (q, $^1J_{C-F}$ 285, CF_3), 126.90 (C1), 127.78, 128.50, 129.17, 130.69, 131.87, 132.28, 132.87, 133.45, 136.66, 136.79, 138.02, 151.12 (C2), 155.25 (q, $^2J_{C-F}$ 42.0, C=O). *m/z* (EI) (%) = 432 (M^+), 303, 252, 251, 221, 220, 207, 206, 133, 132, 91, 57, 41. HRMS Found 432.2281, required for $C_{26}H_{31}O_2F_3$: 432.2276.

2,2-Dimesityl-1-phenylethenyltrifluoroacetate (T2). 2,2-Dimesityl-1-phenylethenol (E2) (0.60 g, 1.5 mmol), pyridine (2.0 g, 13 mmol) and trifluoracetic anhydride (1.5 g, 7.1 mmol) yielded 0.60 g (1.2 mmol, 80%) of **T2** as a white solid. Mp 160 °C (Found: C, 74.1; H, 6.1. $C_{28}H_{27}O_2F_3$ requires: C, 74.3; H, 6.0%). IR (KBr): ν/cm^{-1} = 2960 (C–H), 1785 (C=O), 1605 (C=C), 1440, 1365, 1235, 1180–1140, 850, 770, 755, 695. δ_H($CDCl_3$) 1.80 (br, 3 H, *o*-CH_3), 2.02 (br, 6 H, *o*-CH_3), 2.20 (s, 3 H, *p*-CH_3), 2.22 (s, 3 H, *p*-CH_3), 2.48 (br, 3 H, *o*-CH_3), 6.70 (br, 2 H, mesityl-H), 6.84 (br, 2 H, mesityl-H), 7.06 (m, 2 H, Ph-H), 7.18 (m, 3 H, Ph-H). δ_C($CDCl_3$) 20.10 (br), 20.85, 20.95 (br), 114.44 (q, $^1J_{C-F}$ 285, CF_3), 128.19, 128.31 (br), 128.57 (br), 128.90, 129.61 (br), 129.75, 132.28, 133.38, 133.70, 137.35, 137.97 (br), 144.25 (C1), 155.71 (q, $^2J_{C-F}$ 42.4, C=O). *m/z* (EI) = 453, 452 (M^+), 355, 341, 340, 327, 325, 323, 220, 219, 207, 105, 91, 77. HRMS Found: 452.1964, required: 452.1963.

Cyclic voltammetry

In a glove box tetra(butyl)ammoniumhexafluorophosphate (232 mg, 600 μmol) and the electroactive species (6 μmol) were placed into a thoroughly dried CV cell. At a high purity argon line acetonitrile or dichloromethane (6.0 cm^3) was added through a gas-tight syringe, then a 1 mm platinum disc electrode as working electrode, a Pt wire counter electrode and a Ag pseudo reference electrode were placed into the solution. The cyclic voltammograms were recorded at various scan rates using various starting and switching potentials. For determination of the oxidation potentials, ferrocene was added as the internal standard. CVs were recorded using a Princeton Applied Research Model 362 potentiostat with a Philips model PM 8271 XYt-recorder for scan rates <1 V s^{-1}. For fast scan cyclic voltammetry, a Hewlett Packard model 331A4 function generator was used connected to a three-electrode potentiostat developed by Amatore.[21] The ratios I_{pc}/I_{pa} were determined according to the equation of Nicholson.[22]

Digital simulations of the cyclic voltammograms

The computer simulations of the cyclic voltammetry were carried out on a 486DX66 computer using the Crank–Nicholson technique[23] and DigiSim.[10] The simulation of a full-cycle voltammogram consisted of 1000 data points, allowing for an acceptable resolution of the cyclic voltammograms. All chemical reactions were assumed to be irreversible except the ET equilibria. With a standard heterogeneous electron transfer constant of k^0_{hetero} = 1 cm s^{-1} and standard diffusion coefficients of $D = 10^{-5}$ cm^2 s^{-1}, the rate constants for the chemical reaction steps were varied to achieve the best possible agreement with the experimental curves.

One-electron oxidation of T2; synthesis of P2

In a glove-box were placed 50.0 mg (111 μmol) of **T2** and 158 mg (220 μmol) of tris(4-nitrophenyl)aminium hexachloroantimonate into two separate test tubes equipped with stirring rods. At a high-purity argon line, 8 cm^3 of acetonitrile was added to each test tube to dissolve the reactants. The solution of the oxidant was added dropwise through a syringe to the solution of **T2**. After stirring overnight, the mixture was quenched with 5 cm^3 of saturated aqueous $NaHCO_3$ and diluted with 15 cm^3 of dichloromethane. The aqueous layer was extracted three times with dichloromethane, and the combined organic layers were washed with saturated NaCl and water and dried over Na_2SO_4. Removal of the solvent afforded the crude product. Column chromatography with cyclohexane–dichloromethane (4:1) afforded **P2** as a white solid. IR $\tilde{\nu}$/cm^{-1} 3469, 2962, 2920, 1616, 1585, 1444, 1208, 1057, 1034, 768. δ_H($CDCl_3$) 1.78 (s, 3 H, CH_3), 1.93 (s, 6 H, *o*-mesityl-CH_3), 2.36 (s, 3 H, CH_3), 2.42 (s, 3 H, CH_3), 2.85 (s, 3 H, CH_3), 5.12 (s, 1 H, OH), 7.00 (s, 2 H, mesityl-H), 7.03 (s, 1 H, Ar-H), 7.54 (m, 2 H, Ar-H), 8.28 (m, 1 H, Ar-H), 8.49 (m, 1 H, Ar-H). HRMS Found: 354.1989. $C_{26}H_{26}O$ requires: 354.1984. E_{pa} (CH_3CN, 0.1 M Bu_4NPF_6, 100 mV s^{-1}) = 0.59 V *vs.* Fc.

Electrolysis of T1

Under an atmosphere of dry argon, 13.5 mg (31.2 μmol) of **T1** and 167 mg (432 μmol) of Bu_4NPF_6 were dissolved in 4.0 cm^3 of acetonitrile. After adding 0.5 cm^3 of trifluoracetic acid, the mixture was electrolysed in an undivided cell at 2.0 V *vs.* Ag at a Pt wire. After 30 min the electrolysis was stopped and the mixture was extracted three times with pentane. The pentane layers were combined and the solvent was removed to yield 7.2 mg (16 μmol, 51%) of unreacted **T1** and 3.4 mg (10 μmol, 32%) of **B1**. The benzofuran derivative **B1** was identified by comparison of the ^{1}H NMR data with those of an authentic sample.[15]

Electrolysis of T2

Under an atmosphere of dry argon, 32.0 mg (70.7 μmol) of **T2** and 380 mg (982 μmol) of Bu_4NPF_6 were dissolved in 8.0 cm^3 of acetonitrile. Then 0.2 cm^3 of trifluoroacetic acid was added. The oxidation potential of **T2** was determined *versus* the applied Ag pseudo reference electrode (E_{pa} = 1.50 V) and the mixture was then electrolysed at 1.6 V *vs.* Ag at a Pt wire. After approximately 65% conversion, the electrolysis was stopped and 20 cm^3 of dichloromethane was added. The aqueous layer was extracted three times with dichloromethane and the combined organic layers were washed with saturated $NaHCO_3$ and water and dried over $MgSO_4$. The solvent was removed and the crude product was extracted with pentane to separate from the electrolyte. The pentane layers were combined and the solvent was removed. From the crude mixture, ^{1}H NMR data for **PT2** were obtained, which was identified by comparison with the authentic compound prepared by esterification of **P2**. δ_H($CDCl_3$) 1.83 (s, 3 H, CH_3), 2.32 (s, 3 H, CH_3), 2.47 (s, 3 H, CH_3), 2.88 (s, 3 H, CH_3), 6.87 (br, 2 H, mesityl-H), 7.11 (s, 1 H, Ar-H), 7.57 (m, 2 H, Ar-H), 7.74 (m, 1 H, Ar-H), 8.54 (m, 1 H, Ar-H). The *o*-mesityl-CH_3 protons were affected by coalescence phenomena and displayed no sharp signal. The aromatic signals were partially superimposed by signals of unreacted **T2**. The crude product was stirred with KOH–ethanol for 2 h, neutralized with saturated NH_4Cl and the aqueous layer was extracted three times with diethyl ether. The combined organic layers were dried over $MgSO_4$ and the solvent was removed. Column chromatography (SiO_2, cyclohexane–dichloromethane) (2:1, R_f = 0.47) afforded pure **P2** (5.0 mg, 14 μmol, 20%) as a white solid, which exhibited the same spectroscopic data as the product obtained from one-electron oxidation.

Acknowledgements

We gratefully acknowledge the financial support by the Volkswagenstiftung and by the SFB 347. In addition, we are most indebted to the Fonds der Chemischen Industrie for the continuous support for our research. We thank Degussa for a generous gift of electrode materials.

References

1 (*a*) P. Maslak, W. H. Chapman, T. M. Vallombroso and B. A. Watson, *J. Am. Chem. Soc.*, 1995, **117**, 12 830; (*b*) P. Maslak and J. N. Narvaez, *Angew. Chem.*, 1990, **102**, 302; *Angew. Chem., Int. Ed. Engl.*, 1990, **29**, 283; (*c*) F. D. Saeva, *Top. Curr. Chem.*, 1990, **156**, 59.

2 M. Schmittel, J. Heinze and H. Trenkle, *J. Org. Chem.*, 1995, **60**, 2726.

3 (*a*) M. Schmittel, M. Keller and A. Burghart, *J. Chem. Soc., Perkin Trans. 2*, 1995, 2327; (*b*) M. Schmittel and R. Söllner, *Angew. Chem.*, 1996, **108**, 2248; (*c*) M. Schmittel and H. Trenkle, to be published.
4 P. G. Gassman and J. Bottorf, *J. Org. Chem.*, 1988, **53**, 1097.
5 (*a*) M. Schmittel and M. Levis, *Chem. Lett.*, 1994, 1939; (*b*) B. B. Snider and T. Kwon, *J. Org. Chem.*, 1992, **57**, 2399; (*c*) B. B. Snider and T. Kwon, *J. Org. Chem.*, 1990, **55**, 4786; (*d*) A. Heidbreder and J. Mattay, *Tetrahedron Lett.*, 1994, **33**, 1973; (*e*) E. Baciocchi, A. Casu and R. Ruzziconi, *Tetrahedron Lett.*, 1989, **30**, 3707; (*f*) Y. Kohno and K. Narasaka, *Bull. Chem. Soc. Jpn.*, 1995, **68**, 322.
6 M. Schmittel and M. Röck, *Chem. Ber.*, 1992, **125**, 1611.
7 E. B. Nadler and Z. Rappoport, *J. Am. Chem. Soc.*, 1987, **109**, 2122.
8 M. Schmittel and U. Baumann, *Angew. Chem.*, 1990, **102**, 571; *Angew. Chem., Int. Ed. Engl.*, 1990, **29**, 541.
9 R. S. Nicholson and I. Shain, *Anal. Chem.*, 1964, **36**, 706.
10 (*a*) M. Rudolph, D. P. Reddy and S. W. Feldberg, *Anal. Chem.*, 1994, **66**, 589A; (*b*) M. Rudolph, *J. Electroanal. Chem. Interfacial Electrochem.*, 1992, **338**, 86.
11 M. Röck and M. Schmittel, *J. Chem. Soc., Chem. Commun.*, 1993, 1739.
12 L. L. Miller, G. D. Nordblom and E. A. Mayeda, *J. Am. Chem. Soc.*, 1972, **37**, 1739.
13 P. G. Gassman and R. Yamaguchi, *J. Am. Chem. Soc.*, 1979, **101**, 1308.
14 M. J. S. Dewar, E. G. Zoebisch, E. F. Healy and J. J. P. Stewart, *J. Am. Chem. Soc.*, 1985, **107**, 3902.
15 M. Röck and M. Schmittel, *J. Prakt. Chem.*, 1994, **336**, 325.
16 (*a*) D. F. Unterecker and S. Bruckenstein, *Anal. Chem.*, 1972, **44**, 1009; (*b*) D. F. Unterecker and S. Bruckenstein, *J. Electroanal. Chem. Interfacial Electrochem.*, 1974, **57**, 77.
17 (*a*) D. J. Kuchynka and J. K. Kochi, *Inorg. Chem.*, 1988, **27**, 2574; (*b*) K. Hinkelmann, J. Heinze, H.-T. Schacht, J. S. Field and H. Vahrenkamp, *J. Am. Chem. Soc.*, 1989, **111**, 5078.
18 J. Heinze, *Angew. Chem.*, 1984, **96**, 823; *Angew. Chem., Int. Ed. Engl.*, 1984, **23**, 831.
19 (*a*) P. Maslak and S. L. Asel, *J. Am. Chem. Soc.*, 1988, **110**, 8260; (*b*) P. Maslak, T. M. Vallombroso, W. H. Chapman, Jr. and J. N. Narvaez, *Angew. Chem.*, 1994, **106**, 110; *Angew. Chem., Int. Ed. Engl.*, 1994, **33**, 73.
20 O. Takahashi and O. Kikuchi, *Tetrahedron Lett.*, 1991, **32**, 4933.
21 C. Amatore, C. Lefrou and F. Pflügler, *J. Electroanal. Chem. Interfacial Electrochem.*, 1989, **270**, 43.
22 R. S. Nicholson, *Anal. Chem.*, 1966, **38**, 1406.
23 (*a*) A. Lasia, *J. Electroanal. Chem. Interfacial Electrochem.*, 1983, **146**, 397; (*b*) J. Heinze, M. Störzbach and J. Mortensen, *J. Electroanal. Chem. Interfacial Electrochem.*, 1984, **165**, 61; (*c*) J. Heinze and M. Störzbach, *J. Electroanal. Chem. Interfacial Electrochem.*, 1993, **346**, 1.

Paper 6/02884E
Received 24*th April* 1996
Accepted 16*th July* 1996